NASA Technical Memorandum 88957

Resistojet Plume and Induced Environment Analysis

(NASA-TM-88957) RESISTOJET PLUME AND INDUCED ENVIRONMENT ANALYSIS P.S. Thesis - Case Western Reserve Univ. (NASA) 60 p
Avail: NTIS HC A04/MF A01 CSCL 21H G3/20

N87-24536
Unclas
0083767

David J. Hoffman
Lewis Research Center
Cleveland, Ohio

May 1987

NASA

RESISTOJET EXHAUST PLUME AND INDUCED ENVIRONMENT ANALYSIS

David J. Hoffman
National Aeronautics and Space Administration
Lewis Research Center
Cleveland, Ohio 44135

E-3410

SUMMARY

The source flow method developed by G.A. Simons for calculating the far field plume density produced by high thrust rocket nozzles is modified and applied to low thrust resistojet nozzles with Reynolds numbers on the order of 4000 to 7000. Simons' original method and the modified analysis are compared to mass flux measurements taken by Chirivella in a JPL vacuum tank facility. Results of the comparison show the modified analysis presented in this paper more accurately predicts the mass flux at large angles from the nozzle centerline than Simons' original method. The modified Simons analysis is then used to calculate the plume structure and two contamination parameters, number column density and back flow, for five nozzle geometries representative of space station resistojets.

TABLE OF CONTENTS

	Page
Summary	1
Symbols	iii
Introduction	1
Plume Analysis	3
Boundary Layer Analysis	16
Comparisons With Data in the Literature	20
Discussion	23
Induced Environment Analysis	26
Parametric Studies on NCD and Estimated Back Flow	31
References	40
Tables	44
Figures	46

SYMBOLS

A	plume normalization constant also, constant in Cohen/Reshotko boundary layer analysis
Av	Avogadro's number, 6.02×10^{23}
a_o	sonic velocity at stagnation conditions
B	constant in Cohen/Reshotko boundary layer analysis
d	horizontal distance between source and observer in induced environment analysis
F	function relating the Mach number in the nozzle to the nozzle area ratio
H	form factor, δ^*/θ
H_{tr}	transformed form factor
$\underline{h}$	vector from source location to observer location in induced environment analysis
K	constant used in equation (16) for β
k	constant used in equation (28)
L	nozzle wall length
ℓ	vertical distance between source and observer in induced environment analysis
M	Mach number
M_e	Mach number at nozzle exit also, Mach number external to boundary layer
MW	molecular weight
m	mass flow rate
n	correlation number in Cohen/Reshotko boundary layer analysis

P_o	stagnation pressure
p	point in space along a line of sight
R	nozzle radius in boundary layer analysis
r, $\underline{r}$	polar coordinate radial distance from point source in plume density equations
r^*	nozzle throat radius
r_e	nozzle exit radius
S_w	wall enthalpy function
$\underline{s}$	line of sight vector originating from observer location
T_o	stagnation temperature
T_w	nozzle wall temperature
U	gas velocity
$\bar{U}$	average gas velocity
U_l	average limiting gas velocity for fluid from the nozzle boundary layer
x	distance along nozzle wall
x_l	nozzle length
α	constant in the equation for U_l
β	constant in exponential plume equation
γ	specific heat ratio
δ	boundary layer thickness
δ^*	displacement thickness
δ_{tr}	transformed boundary layer thickness
ζ	Sutherland's constant
ν	Prandtly-Meyer angle

θ polar coordinate angle from centerline in plume density equations also, momentum thickness in boundary layer analysis

θ_b back flow angle

θ_l limiting expansion angle

θ_o angle which boundary layer streamline turns through

θ_∞ the value of θ_l for inviscid supersonic flow

$\theta_{\infty(l)}$ limiting turning angle for subsonic inviscid flow

θ_{tr} transformed momentum thickness

λ viscosity law constant

μ angle in space station induced environment analysis

ν_o kinematic viscosity at l_o

ρ density

ϕ line of sight angle

Ω solid angle

Subscripts

b back flow

e nozzle exit conditions

l limiting value

noz nozzle

o stagnation conditions

∞ limiting value

Superscripts

* sonic conditions

Abbreviations

LOS	line of sight
mol	molecules
NCD	number column density
QCM	quartz crystal microbalance

INTRODUCTION

The induced environment is defined as the environment which is produced by the presence and operation of a spacecraft. This includes molecules, particulates, electric fields, etc. emitted or created by the space structure. The detrimental effects of contamination from propulsion systems and various other sources have been seen on numerous manned and unmanned missions [1]. In the past, contamination from the induced environment was an afterthought in the design of spacecraft systems. With the development of increasingly sensitive astronomical instruments such as the Space Infrared Telescope Facility [2] and the advent of the space station which may be degraded by the effects of contamination, designers of space systems are paying more attention to the identification and modeling of contamination sources and their effects.

An electrothermal propulsion system, commonly known as the resistojet since it uses electrical resistance to heat a gas and expand it through a nozzle, will be used on the NASA space station to provide orbit maintenance as well as waste gas disposal. A concern with this system, as with any propulsion system, is its impact on the space station environment due to the exhaust plume. In analyzing contamination from plumes, the prediction of the plume structure itself is a key element and is very difficult to do quickly and accurately. Once the plume structure is known the contamination parameters can be assessed.

The first portion of this report is devoted to modifying a closed form source flow method for prediction of the far field plume density developed by G. A. Simons [3] for application to the viscous flowfield produced by resistojet thrusters. The original Simons method has been applied to small thrusters with large viscous effects [4 through 10]. The different results for the plume parameters obtained using the original and modified Simons methods are pointed out in this paper. In carrying out the plume analysis, the boundary layer and displacement thicknesses must be known at the rocket nozzle exit. Therefore, the following section describes the boundary layer modeling used. Next, the plume analysis developed in this report is compared to data from reference 26.

The second portion of the report presents the results of a parametric study assessing the induced environment for five cases representing typical space station resistojet geometries and operating conditions. This study uses the results of the plume analysis section to predict two induced environment parameters, column density and back flow. The analysis is followed by a discussion of the results.

PLUME ANALYSIS

Perhaps the most critical aspect of a contamination analysis of a propulsion system entails the determination of the exhaust plume structure. For the Reynolds number range (typically 4000-7000) found in resistojet thrusters, this task is difficult. Method-of-characteristics computer codes used to analyze the higher thrust engines (greater than 5 lb_f) need modification to accurately model the more viscous flow in nozzles of less than 100 mlb_f thrusters [11 and 12]. The viscous nozzle flow field can be analyzed by a Navier-Stokes routine while the vacuum free expansion is best modeled by a Direct Simulation Monte-Carlo method [13 to 16], but these techniques are time consuming and expensive. There exist source flow representations of rocket nozzle exhaust plumes valid in the far field which are easily and quickly applied once the nozzle geometry and operating conditions are known [3, and 18 to 22].

In this paper, a closed form source flow method devised by G.A. Simons [3] is modified to model resistojet thruster flow fields. Simons' method is a generalization of the numerical results obtained by Boynton for rocket engines with thrusts greater than 10 lb_f [17]. Boynton calculates exhaust plume flow fields from nozzles with boundary layer effects using a finite difference numerical scheme in which the expansion of rotational supersonic fluid around the nozzle lip is treated inviscidly and the subsonic portion of the boundary layer is neglected.

Large differences in the far field plume structure, especially at large angles from the plume centerline, are found when the supersonic portion of the boundary layer is included. Simons generalized Boynton's results by expressing the plume properties in terms of the boundary layer thickness and nozzle exit conditions. Difficulties arise in applying these methods to lower thrust devices such as resistojets because the boundary layer at the nozzle exit plane is a large percentage of the exit plane radius, a condition neglected in previous analyses. Simons' method is modified in this present work by retaining a higher order term, involving the ratio of the boundary layer thickness to the nozzle exit radius, in the development of the equation for plume density. Some of Simons' simplifying expansions are not made in the modified analysis for the resistojet nozzle flows. A review of the development of the original Simons method and its modifications are presented below.

In the far field, the flow from the rocket nozzle behaves as if it is diverging radially from a point source, as depicted in figure 1. The continuity equation is used to relate the mass flux in the plume to the mass flux at the throat of the nozzle. Assuming the local density is related to the plume centerline density by a function $f(\theta)$,

$$\rho(r,\theta) = \rho(r,\theta = 0)f(\theta), \qquad (1)$$

the continuity equation becomes

$$\rho^* U^* \pi r^{*2} = \rho(r, \theta = 0) U_1 \int_0^{\theta_1} 2\pi r^2 f(\theta) \sin\theta d\theta \qquad (2)$$

Where θ_1 is the limiting turning angle of the gas at the nozzle exit plane and is calculated by taking the difference between the Prandtl-Meyer angles for an infinite Mach number expansion and for the Mach number at the exit plane and adding the nozzle half angle.

$$\theta_1 = \nu_{M=\infty} - \nu_{M=Me} + \theta_{noz} \qquad (3)$$

U_1 is the limiting velocity of the gas corresponding to an expansion of the gas to zero static pressure.

$$U_1 = \left(\frac{\gamma + 1}{\gamma - 1}\right)^{1/2} U^* \qquad (4)$$

Simons defines the normalization constant A as,

$$A = \frac{U^*}{2U_1} \left\{ \int_0^{\theta_1} f(\theta) \sin(\theta) d\theta \right\}^{-1} \qquad (5)$$

Using equations (1) and (5) in (2) and rearranging gives the equation for gas density in the far field as

$$\frac{\rho(r,\theta)}{\rho^*} = A\left(\frac{r^*}{r}\right)^2 f(\theta) \qquad (6)$$

Various researchers [18 to 22] have devised several functions for $f(\theta)$ to account for the variation of density with angle from the plume centerline for inviscid flows. Simons follows Boynton's choice [23] of a cosine power function for $f(\theta)$ which obeys the

locally two-dimensional Prandtl-Meyer expansion function for θ near θ_1.

$$f(\theta) = \left\{\cos\left(\frac{\pi}{2}\,\frac{\theta}{\theta_\infty}\right)\right\}^{2/(\gamma-1)} \tag{7}$$

where θ_∞ is the value of θ_1 for inviscid supersonic flow. This cosine power function correlates well with Boynton's numerical results for the far field plume structure for inviscid nozzle flow. However, when the effects of the supersonic boundary layer in the nozzle and its subsequent expansion into the far field are considered, Boynton notes large discrepancies from the angular dependency given by equation (7) for θ near θ_∞. In fact the decrease in density with increasing angle from the plume centerline follows an exponential decay. Simons proposes a second function for $f(\theta)$ to be used for angles greater than an angle θ_0 such that

$$f(\theta) = f(\theta_0)\exp[-\beta(\theta - \theta_0)] \tag{8}$$

where it is assumed that the boundary layer streamline turns through the angle θ_0, and θ_0 and β are functions of the nozzle exit conditions. In this way, the far field plume structure is modeled by two equations: (1) a cosine power law valid from $\theta = 0$ to $\theta = \theta_0$ which models the expansion of the fluid from the inviscid core of the nozzle, and 2) an exponential function valid from $\theta = \theta_0$ to $\theta = \theta_\infty$ which models the expansion of the fluid coming from the nozzle boundary layer. The plume is assumed to be axisymmetric. To calculate the far

field plume structure, the values for A, ß, and θ_o are calculated. As stated above, ß and θ_o are determined by the nozzle exit conditions. The means for calculating A is given below.

If it is initially assumed that the nozzle flow is entirely inviscid, the far field plume shape is governed by the cosine function, equation (7). Using equations (7) and (4) in equation (5), A is calculated as

$$A = \left(\frac{\gamma + 1}{\gamma - 1}\right)^{1/2} \frac{\pi^2}{8\theta_\infty^2} \quad . \tag{9}$$

In evaluating the integral in equation (5), the approximation

$$\sin\theta = \left(\frac{2\theta_\infty}{\pi}\right) \sin\left(\frac{\pi}{2}\right)\left(\frac{\theta}{\theta_\infty}\right) \tag{10}$$

is used. The parameters θ_o and ß are related to the ratio of the boundary layer thickness to nozzle radius at the exit plane by using conservation of mass.

The development of the plume density equations given above has been a review of Simons' work based on Boynton's results. The following analysis for determining θ_o and ß is a result of modifications to Simons' original work in an effort to make the method more accurate for cases where the ratio of the boundary layer thickness to the nozzle radius at the exit plane is not small, as is the case for most resistojet flowfields.

The value for θ_o, which is the angle from the centerline of the streamline which separates the inviscid core flow from the

flow in the boundary layer, is determined by equating the mass flow in the inviscid core of the nozzle with the mass flow in the plume found within a symmetrical cone of half angle θ_0,

$$\rho_e U_e \pi (r_e - \delta)^2 = \int_0^{\theta_0} 2\pi \rho U_1 r^2 \sin\theta d\theta \quad . \tag{11}$$

The integral is evaluated using the approximation given by equation (10), substituting equation (6) for ρ using equation (7) for $f(\theta)$ since this is the expansion of the fluid from the inviscid core of the nozzle, and substituting equations (4) and (9) for U_1/U^* and A, respectively. After some rearrangement, the equation for $f(\theta_0)$ is given as

$$f(\theta)_0 = \left\{ \cos \left(\frac{\pi}{2} \frac{\theta_0}{\theta_\infty} \right) \right\}^{2/(\gamma-1)} = \left[\frac{\delta}{r_e} \left(2 - \frac{\delta}{r_e} \right) \right]^{2/(\gamma+1)} \quad . \tag{12}$$

Solving the above equation for θ_0/θ_∞

$$\frac{\theta_0}{\theta_\infty} = \left(\frac{2}{\pi} \right) \cos^{-1} \left\{ \left[\frac{\delta}{r_e} \left(2 - \frac{\delta}{r_e} \right) \right]^{(\gamma-1)/(\gamma+1)} \right\} \quad . \tag{13}$$

Equations (11), (12), and (13) differ from those of Simons. Since he was studying cases where the boundary layers were small compared to the nozzle exit radius and the expansion angle θ_0 approaches θ_∞, he was able to neglect the δ^2 term in equation (11) and expand the cosine function in equation (12) in a Taylor series for θ_0 near θ_∞. It is more accurate to solve for θ_0/θ_∞ directly instead of introducing further approximations. Although Simons arrived at his equations for $f(\theta_0)$ and θ_0/θ_∞ by

equating the nozzle boundary layer mass flow to the mass flow in the plume diverging at angles greater than θ_0, the end results are equivalent to the results given by equations (12) and (13) since the plume normalization constant is defined the same way. Simons' forms of equations (12) and (13) are duplicated below.

$$f(\theta_0) = \left\{ \cos\left(\frac{\pi}{2}\right)\left(\frac{\theta_0}{\theta_\infty}\right)\right\}^{2/(\gamma-1)} = \left(\frac{2\delta}{r_e}\right)^{2/(\gamma+1)} \tag{12S}$$

$$\frac{\theta_0}{\theta_\infty} = 1 - \left(\frac{2}{\pi}\right)\left(\frac{2\delta}{r_e}\right)^{(\gamma-1)/(\gamma+1)} \tag{13S}$$

Once the $(\delta/r_e)^2$ term in the far right hand side of equation (12) is neglected and the cosine function expanded into a Taylor series, these results reduce to Simons' original forms, equations (12S) and (13S). The final parameter to be determined is the constant β.

Once again using continuity and assuming the boundary layer mass flow expands inviscidly from initial viscous conditions, a relationship between the fluid expanding in the plume beyond the angle θ_0 and the boundary layer fluid is written as

$$2\pi r_e U_e \rho_e \delta - \rho_e U_e \pi \delta^2 = \int_{\theta_0}^{\theta_\infty} 2\pi \rho \bar{U}_1 r^2 \sin\theta d\theta \tag{14}$$

where the δ^2 term is retained. The integral is evaluated by using equation (6) for ρ and equation (8) for $f(\theta)$ since the

gas in this region follows the exponential angular dependency. $\bar{U}_1$ is the average limiting velocity in the far field of the fluid from the supersonic boundary layer in the nozzle and becomes a constant of integration ($\bar{U}_1 = \alpha U_1$ where $0.5 \leq \alpha \leq 1.0$). After evaluating the integral, dividing both sides of the equation by $\rho_e U_e r_e^2$, and assuming $\exp(-\beta\theta_\infty) = 0$

$$\frac{\delta}{r_e}\left(2 - \frac{\delta}{r_e}\right) = \frac{2A\rho^* r^{*2} \bar{U}_1}{\rho_e U_e r_e^2}\left[\frac{\delta}{r_e}\left(2 - \frac{\delta}{r_e}\right)\right]^{2/(\gamma+1)} \times \left\{\frac{\beta\sin\theta_o + \cos\theta_o}{\beta^2 + 1}\right\} \qquad (15)$$

At this point, besides neglecting the term $(\delta/r_e)^2$, Simons assumes $\beta >> 1$ and $\sin\theta_o$ is approximately $O(1)$ which are valid approximations for nozzles with relatively small boundary layers. In the present analysis, the above assumptions are not made resulting in the following expression for β

$$\beta = \frac{K}{2}\sin\theta_o + \sqrt{\frac{K^2}{4}\sin^2\theta_o + K\cos\theta_o - 1} \qquad (16)$$

where K is

$$K = A\left(\frac{\gamma+1}{\gamma-1}\right)^{1/2} \frac{2\bar{U}_1}{U_1}\left[\frac{\delta}{r_e}\left(2 - \frac{\delta}{r_e}\right)\right]^{(1-\gamma)/(\gamma+1)}$$

Whereas Simons' equation for β is written as

$$\beta = A\left(\frac{\gamma+1}{\gamma-1}\right)^{1/2}\left(\frac{2\bar{U}_1}{U_1}\right)\left(\frac{r_e}{2\delta}\right)^{(\gamma-1)/(\gamma+1)} \qquad (16S)$$

If Simons' simplifying assumptions are used, equation (16) will reduce to equation (16S), as expected.

To see what the effect of using the simplifying assumptions employed by Simons which are valid for nozzles with thin boundary layers, values for $f(\theta_0)$, θ_0, and β are computed using equations (12), (13) and (16) compared to equations (12S), (13S) and (16S).

Assume $\gamma = 1.3$, $M_e = 5.0$, $\delta/r_e = 0.20$, and $\theta_{noz} = 20°$. Then from equation(3) $\theta_1 = \theta_\infty = 90°$ and from equation (9) $A = 1.38$. Using Simons' equation for $f(\theta_0)$,

$$f(\theta_0) = \left(\frac{2\delta}{r_e}\right)^{2/(\gamma+1)}$$

with $\delta/r_e = 0.2$ results in $f(\theta_0) = 0.45$. Simons' equation for θ_0/θ_∞ (equation (13S)) gives $\theta_0 = 39°$. From equation (16S), the value for β is 6.46, assuming $\bar{U}_1 = 0.75U_1$.

Using the present analysis, equation (13) yields $\theta_0 = 29°$ which is 10° smaller than that calculated above. The lower value of θ_0 calculated using the modified analysis shows that the thicker boundary layer at the nozzle exit plane inhibits the streamline at the edge of the boundary layer from expanding as far as it will if Simons' original analysis, which does not retain the higher order boundary layer terms, is used. The calculation using equation (12) gives $f(\theta_0) = 0.41$. Finally, $\beta = 4.28$ from equation (16). Since β is the constant in the exponential function describing the variation in gas density as a function of

θ, the lower value given by the present analysis as compared to Simons' original means that the gas density decays less rapidly with increasing angle. Physically, this is a result of the thicker boundary layers in the nozzle.

The equations and parameters developed above for calculating the far field plume density structure depend on the nozzle physical characteristics (θ_{noz}, r^*, r_e), type of propellant (γ), and flow conditions (ρ^*, δ, θ_∞).

The calculation of the nozzle flow conditions are outlined below and in the next section. The Prandtl-Meyer expansion angle θ_∞ is a function of γ, M_e and θ_{noz}. The Mach number at the nozzle exit is a function of γ and the effective nozzle area ratio, based on a one-dimensional isentropic expansion. The boundary layer displacement thickness at the exit plane reduces the physical nozzle area ratio which in turn reduces the exit Mach number. The next section describes how the nozzle boundary layer parameters and exit Mach number are calculated. Once M_e and the stagnation chamber conditions (P_o,T_o) are known, other state parameters in the nozzle core flow are determined using the one-dimensional isentropic relations.

The equations for the far field plume density derived above assume all of the gas from the nozzle is contained within a symmetrical cone with a half angle of θ_∞. The angle θ_∞ is calculated to be the limiting Prandtl-Meyer expansion angle (plus θ_{noz}) for supersonic core flow corresponding to

γ and M_e. As seen by equation (13), nozzle viscous effects prevent the supersonic core fluid at the edge of the boundary layer from expanding to θ_∞. Instead, the supersonic boundary layer fluid expands from θ_0 out to θ_∞. In reality, the boundary layer contains fluid travelling at supersonic and subsonic velocities. As shown by Bird [13], the subsonic fluid accelerates to $M = 1$ at the nozzle lip. The $M = 1$ flow at the nozzle lip will expand to the Prandtl-Meyer angle given by

$$\theta_\infty(1) = \nu_{Me=\infty} - \nu_{Me=1} + \theta_{noz} = \left(\left(\frac{\gamma + 1}{\gamma - 1}\right)^{1/2} - 1\right) \times 90^\circ + \theta_{noz} \qquad (17)$$

From the equation for θ_∞ (1) above and equation (3), it is seen that the subsonic portion of the boundary layer expands beyond θ_∞. Boynton and Simons both neglected the behavior of the subsonic portion of the boundary layer stating that only a small portion of the total mass flow is contained within it.

It is known that physically, there is no sharply defined cut off angle θ_∞ beyond which there is zero mass flow. Direct Simulation Monte Carlo calculations [13 to 16] analyzing the nozzle lip phenomenon show there is back flow even at angles 180° from the plume centerline. From a continuum point of view, the entire boundary layer flow will expand beyond θ_0, filling the region from θ_0 to $\theta_\infty(1)$. The supersonic boundary layer fluid will expand to somewhere near or beyond θ_∞ while the subsonic portion will expand beyond θ_∞ out to $\theta_\infty(1)$. In an attempt to refine the source flow method presently described, it may be proposed to account for the expansion of the boundary

layer fluid from an angle θ_1' out to $\theta_\infty(1)$. Doing this would be equivalent to finding the angle θ_1' in the far field where the initially subsonic fluid is encountered. This can not readily be done for the following reasons. The plume constant A defined by equation (5) has an integral evaluated from $\theta = 0$ to $\theta = \theta_1 = \theta_\infty$ within which all the mass flow is contained by definition. To be consistent with Boynton's choice for $f(\theta)$ given by equation (7) which is derived from a large Mach number expansion of the Prandtl-Meyer function, the angle θ_∞ must be defined as in equation (3). Finally, the boundary layer parameters at the nozzle exit plane calculated by the method discussed in the next section are not of sufficient detail to accurately calculate the subsonic boundary layer mass flow or Mach number profiles. For these reasons along with the assumption that the mass flow in it is small, the behavior of the subsonic portion of the boundary layer is neglected although the entire mass flow in the boundary layer is accounted for by continuity. In this way the effect of both the subsonic and supersonic portions of the boundary layer on the plume is "smeared out". For the present analysis, it is also assumed that θ_∞ is the limiting expansion angle beyond which there is negligible mass flow. In summary then, as depicted in figure 1 the far field plume density is modeled by the following two equations:

$$0 \le \theta \le \theta_0 \qquad \frac{\rho}{\rho^*} = A\left(\frac{r^*}{r}\right)^2 \left[\cos\left(\frac{\pi}{2}\right)\left(\frac{\theta}{\theta_\infty}\right)\right]^{2/(\gamma-1)}$$

$$\theta_0 \le \theta \le \theta_\infty \qquad \frac{\rho}{\rho^*} = A\left(\frac{r^*}{r}\right)^2 f(\theta_0)\exp[-\beta(\theta - \theta_0)] \qquad (18)$$

where the constants A, θ_0, θ_∞, and β are given by equations (9), (13), (3), and (16) respectively.

BOUNDARY LAYER ANALYSIS

The nozzle exhaust plume structure in the far field is strongly influenced by the ratio of the nozzle exit boundary layer thickness to the nozzle exit radius. Furthermore, displacement thickness effects reduce the exit Mach number and the corresponding expansion angle θ_∞. For these reasons it is desirable to get a good prediction of the viscous effects at the nozzle exit. Since the boundary layers in resistojet thrusters tend to be laminar, the Cohen-Reshotko method for compressible laminar boundary layers with heat transfer and arbitrary pressure gradient [24] is used.

The Cohen-Reshotko method relates a correlation number n, which is called the pressure gradient parameter, to the boundary layer characteristics. The first step in obtaining the boundary layer parameters at the exit plane is to calculate the correlation number as follows

$$n = - A \frac{M_e^{-B}}{R^2} \frac{dM_e}{d\left(\frac{x}{L}\right)} \left(1 + \frac{\gamma - 1}{2}\right) M_e^{\,2} \quad (3\gamma-1)/(2\gamma-2)$$

$$x \int_0^{x/L} \frac{R^2 M_e^{\,B-1}}{\left(1 + \frac{\gamma - 1}{2} M_e^{\,2}\right) (3\gamma-1)/(2\gamma-2)} \, d\left(\frac{x}{L}\right) \quad . \qquad (19)$$

The number n at the exit depends in part on an integral evaluated from the throat (x/L = 0) to the exit (x/L = 1). There are two functions in the integrand which are the radius of the

nozzle, R, and the inviscid Mach number at the exit, M_e, as they vary with non-dimensional distance x/L along the nozzle wall. The function for R is easily determined. The function $M_e = M_e(x/L)$ is given by "inverting" the one-dimensional isentropic function for area ratio (A_e/A^*) as a function of Mach number

$$\frac{A}{A^*} = \frac{1}{M}\left[\frac{2}{\gamma+1}\left(1 + 0.5(\gamma - 1)M^2\right)\right]^{(\gamma+1)/2(\gamma-1)}. \qquad (20)$$

This is done by finding the zeros by Newton's method of the following function which takes into account the blockage due to the displacement thickness at the exit plane.

$$F = \frac{x}{L} - \left(\frac{x_1}{r_e - r^* - \delta^*}\right)\left(\frac{r^*}{\cos\theta}\right) \times \left\{\sqrt{\frac{1}{M}\left[\frac{2}{\gamma+1}\left(1 + \frac{\gamma-1}{2}M^2\right)\right]^{(\gamma+1)/(2\gamma-2)}} - 1\right\} \qquad (21)$$

The Mach number at any point along the nozzle wall is now known so that the integral in equation (19) can be evaluated. Equation (21) will give the exit Mach number corresponding to the reduction in area ratio due to the displacement thickness. The term $dM_e/d(x/L)$ can be evaluated numerically. The only unknown terms yet to be determined in equation (19) are the constants A and B. These constants depend on the wall enthalpy function S_w,

$$S_w = \frac{T_w}{T_o} - 1, \qquad (22)$$

Where T_w is the wall temperature. It is assumed that $T_w = T_o$ so that $S_w = 0$. Then, on figure 4 of reference 24, a tangent line to the curve of N versus n is drawn at n = -0.105, which is the limiting value of n from exact solutions ($S_w = 0$). The result is that the line $N = A + Bn$ is determined with A = .40 and B = 4.79. The tangent line is drawn at n = -0.105 because strong favorable pressure gradients are found in rocket nozzles of short length. Now that the correlation number n is known, the momentum, displacement and boundary layer thickness are easily determined.

Momentum thickness

$$\theta = \left\{ \left(\frac{\nu_o \lambda L}{a_o} \right) \left(- \frac{n}{\frac{dM_e}{d\left(\frac{x}{L}\right)}} \right) \left(1 + 0.5(\gamma - 1) M_e^2 \right)^{(3-\gamma)/(2\gamma-2)} \right\}^{1/2}$$

where

ν_o kinematic viscosity at T_o

a_o sonic speed at T_o

L characteristic length

$$\lambda = (T/T_o)^{1/2}(T_o + \zeta)/(T + \zeta) \qquad (24)$$

where

ζ is Sutherlands viscosity for air

Displacement thickness

$$\frac{\delta^*}{\theta} = H = H_{tr} + 0.5(\gamma - 1) M_e^2 (H_{tr} + 1) \qquad (25)$$

where

H_{tr} is obtained from figure 7 in [24] or by equation 17 in [25] for adiabatic nozzles.

Boundary layer thickness

$$\frac{\delta}{\theta} = \frac{\delta_{tr}}{\theta_{tr}} + 0.5(\gamma - 1)M_e^2(H_{tr} + 1) \qquad (26)$$

where

δ_{tr}/θ_{tr} is obtained from figure 8 in [24] or by equation 17 in [25] for adiabatic nozzles.

The above calculations are carried out numerically in an iterative process. Given an initial guess for δ^*, the program uses equation (21) and a routine which finds zeroes of a function by a Newton's method to calculate the exit Mach number. The Mach number near the exit plane is calculated so that $(dM/dx)_{x/L = 1}$ can be evaluated numerically. Next, the program calculates the correlation number n at the exit plane after evaluating the integral in equation (21) by a Simpson's rule routine. Once the correlation number is known, the new boundary layer parameters are evaluated. If the new δ^* differs by more than one percent from the δ^* given by the previous iteration, the program loops around and begins the next iteration by calculating the new exit Mach number given by the latest δ^*.

COMPARISONS WITH DATA IN THE LITERATURE

The results for far field density given by equation (18) along with an assumption regarding the limiting velocity of tne gas in the plume as it varies with angle from the plume centerline are used to compute the mass flux per solid angle

$$\frac{d\dot{m}}{d\Omega} = \rho U r^2 \quad . \tag{27}$$

Experimental and numerical results [5] indicate a constant velocity in a core region of the far field plume followed by an exponential decrease in velocity. It is assumed that the constant velocity in the core region for $\theta = 0$ to $\theta = \theta_0$ is the limiting velocity U_1 of the gas for an infinite expansion given earlier by equation (4). Then it is assumed that the ratio U/U_1 decays from unity at $\theta = \theta_0$ to one-half at $\theta = \theta_\infty$ given by

$$\frac{U}{U_1} = \exp[k(\theta - \theta_0)], \quad k = \ln \frac{(0.5)}{(\theta_\infty - \theta_0)} \tag{28}$$

The above equation along with equation (18) are used to evaluate equation (27).

Reference [26] presents a number of figures showing data obtained from quartz crystal microbalance (QCM) measurements in a vacuum chamber of mass flux per unit solid angle versus angular distance from the axis for various rocket nozzles. The values for $dm/d\Omega$ were normalized by centerline values $(dm/d\Omega)_{\theta=0}$ calculated by the Hill and Draper method [18].

In the present analysis, using equations (18) and (28) in equation (27) and normalizing by the centerline value produces

$$[0 \leq \theta \leq \theta_0] \quad \frac{\frac{d\dot{m}}{d\Omega}}{\left(\frac{d\dot{m}}{d\Omega}\right)_{\theta=0}} = \cos\left(\frac{\pi}{2}\,\frac{\theta}{\theta_\infty}\right)^{2/(\gamma-1)} \qquad (29)$$

$$[\theta_0 \leq \theta \leq \theta_\infty] \quad \frac{\frac{d\dot{m}}{d\Omega}}{\left(\frac{d\dot{m}}{d\Omega}\right)_{\theta=0}} = \frac{U}{U_1} f(\theta_0)\exp[\beta(\theta - \theta_0)]$$

$$= f(\theta_0)\exp[(-\beta + k)(\theta - \theta_0)] \qquad (30)$$

where the centerline values used above are given by

$$\left(\frac{d\dot{m}}{d\Omega}\right)_{\theta=0} = \rho^* Ur^{*2} A = \left(\frac{\gamma + 1}{\gamma - 1}\right)^{1/2} (\rho Ur^2)^* A \qquad (31)$$

Results obtained with the original and modified versions of Simons' method, which are presented in table I, were used in equations (29) and (30) to calculate normalized mass flux per solid angle for two cases in reference [26]. The first case is a 15° half angle conical nozzle (nozzle 5) flowing N_2 at $T_0 = 294$ K, $P_0 = 2.19 \times 10^4$ N/m^2. The results are plotted in figure 2 which is a duplicate of figure 16 of reference [26]. The second case is a 25° half angle conical nozzle (nozzle 3) flowing CO_2 at same temperature and pressure as the previous case. The comparison is given in figure 3, a duplicate of figure 13 in reference [26]. It is important to point out that the results for

mass flux per unit solid angle obtained in the present analysis were normalized by the same centerline values given in [26].

DISCUSSION

Figure 2 shows Chirivella's mass flux data for nozzle 5 flowing N_2 taken as far as 140° from the plume centerline. The Hill and Draper approximation, due to the assumption of inviscid nozzle flow, greatly underpredicts the flow at 65° from the nozzle centerline. This angle happens to be the value for $\theta_1 = \theta_\infty$ calculated by equation (3) for Simons' method. As compared to the Hill and Draper approximation, the Simons method calculations show a deficit of mass flux in the core region followed by much greater mass flux values at the larger angles corresponding to the expansion of the nozzle boundary layer. Both versions of Simons' method do a good job in accounting for the mass flux at large angles. The original version of Simons' method slightly underpredicts the mass flux at the limiting angle $\theta_\infty = 65°$ while the modified version slightly overpredicts. The values for θ_0 and β using the original and modified Simons equations are 26° as compared to 18°, and 9.23 compared to 4.67, respectively.

It is interesting to note that the prediction for normalized mass flux using the modified Simons equations extended for angles greater than θ_∞ compares favorably with the data. As mentioned previously, the equations derived in this paper are only strictly valid for angles less than θ_∞. However, it is understood that physically, the expansion of nozzle boundary layer fluid can reach angles much greater than θ_∞. At some angle θ_1', the initially subsonic portion of the boundary layer will

be encountered where exponential given by equation (8) is no longer valid. For reasons stated earlier, the angle θ_1' can not properly be calculated and although the entire boundary layer mass flow is accounted for in a general way, the behavior of the subsonic portion is neglected. Therefore, although not rigorously correct, the exponential behavior of the boundary layer expansion into the far field can be used beyond the limiting angle θ_∞ to get good engineering predictions of the mass flux at large angles.

Figure 3 shows the mass flux data and predictions for Chirivella's nozzle 3, a 25° half angle conical nozzle with a high expansion ratio (240:1) flowing CO_2. Due to the high expansion ratio, inviscid theory predicts a plume which does not spread much, as seen by the Hill and Draper plot. When the boundary layer expansion is taken into consideration, there is again the deficit of mass flux in the core followed by an increase of mass flux at large angles from the centerline. This is seen in the plots for both versions of Simons' method. As in the previous case, the original version of Simons' equations slightly underpredict the mass flux at the angle θ_∞ while modified version overpredicts the expansion. The values for θ_0 are 33° and 18°, and 6.32 and 3.5 for β using the original versus modified Simons, respectively.

Extending the exponential function beyond θ_∞ to get an idea of the mass flux at very large angles from the centerline is

also supported in this case by noting the good comparison of the broken extension for the mass flux prediction using the modified Simons equations.

A comparison of the modified Simons method with recent QCM mass flux data can be found in [27]. The comparison in this reference also shows general agreement between the plume shape given by the modified Simons equations and the data.

The above comparison of the calculations of normalized mass flux using the modified version of Simons' method with experimental data indicate that it can be a powerful tool in systems level studies involving far field plume prediction. The set of equations developed in this paper, following Simons' original development, allow a rapid determination of far field plume density for a wide variety of rocket nozzles even with thick boundary layers.

INDUCED ENVIRONMENT ANALYSIS

In order to predict the induced environment produced by resistojet thruster operation, the structure of the exhaust plume must be known. The means for predicting the far field plume density or normalized mass flux is presented in the Plume Analysis section. Attention is now focused on the analysis which will allow the quantification of the induced environment resulting from resistojet thrusters used by the space station for orbit maintenance/waste gas removal.

The relevant parameters describing the induced environment are number column density, back flow, particulates, and return flux. Number column density (NCD) is defined as the number of molecules per unit area seen by an observer along a specified line of sight (LOS). An observing instrument which experiences a high NCD may have problems clearly seeing its target because the gas producing the high NCD may be absorbing and/or radiating in the wavelengths of interest.

The flow from the rocket nozzle which expands beyond 90° from the plume centerline is called back flow. This can cause problems for sensitive spacecraft surfaces or instruments which can not tolerate deposition of certain species.

If a phase change occurs during the expansion of the propellant gas through the nozzle, particles can be expelled. Particulates impacting spacecraft surfaces may cause problems such

as pitting of windows as well as perturbing observing instruments by scattering sunlight.

It is believed that the resistojet thrusters will not produce particles since the operating conditions (i.e. T_o and P_o) can be manipulated to preclude condensation within the nozzle. For example, the minimum chamber temperature (T_o) for a thruster with a 100:1 area ratio nozzle operating with steam at $P_o = 2.07 \times 10^5$ Pa has to be 300 °C so that a phase change will not occur in the nozzle, based on a one dimensional isentropic expansion. Once outside the nozzle, the mean free path between molecules increases greatly, further reducing the chance of collisions which induce particulate formation.

Return flux is the process of molecular effluent impingement on a surface after colliding with ambient molecules, indicating it is a deposition concern. Return flux will not be addressed since it requires analysis involving molecular collisions which is not covered in this paper.

Once the far field plume density functions are known, the NCD along a given line of sight (LOS) is determined by integrating the induced density from the LOS origin to infinity,

$$NCD = \frac{A_V}{MW} \int_0^\infty \rho \, ds \ [\text{molecules/cm}^2] \qquad (32)$$

where ds is the incremental distance along the LOS.

The situation is depicted in figure 4. The observer and resistojet thruster source are located at the opposite ends of the hypotenuse of a right triangle with legs of lengths ℓ and d, corresponding to the space station with an observing instrument located on the center of the upper boom of the dual keel reference configuration and thrusters located on a "stinger" aft of the modules, as shown in figure 5. In order to evaluate equation (32) on substitution of equation (18) for ρ, expressions for r and θ as functions of distance along the LOS s must be found. In vector notation with the origin taken to be the thruster location, the observer is located at

$$\underline{h} = - d\,\underline{i} + \ell\,\underline{j}$$

while a point p at a distance s along the LOS is found by

$$\underline{s} = |\underline{s}|\cos\varphi\,\underline{i} + |\underline{s}|\sin\varphi\,\underline{j}$$

so that the distance r from the thruster to the point p is

$$|\underline{r}| = |\underline{h} + \underline{s}| = [(|\underline{s}|\cos\varphi - d)^2 + (|\underline{s}|\sin\varphi + \ell)^2]^{1/2} . \tag{33}$$

From figure 4

$$\theta = \cos^{-1}\frac{[(\underline{s} + \underline{h}) \cdot \underline{i})]}{|\underline{r}|} = \cos^{-1}\frac{[(|\underline{s}|\cos\varphi - d)]}{|\underline{r}|} \tag{34}$$

The model for far field density separates the plume into two zones so that it is necessary in evaluating equation (32) to know which equation for ρ to use. From figure 4, the distance s_1

from the observer location to the intersection of the plume boundary θ_∞ is

$$s_1 = |\underline{h}| \frac{\sin(180° - \mu - \theta_\infty)}{\sin(\theta_\infty - \varphi)} \tag{35}$$

and the distance s_2 from the observer to the inviscid core plume boundary θ_0 is

$$s_2 = |\underline{h}| \frac{\sin(180° - \mu - \theta_0)}{\sin(\theta_0 - \varphi)} \tag{36}$$

where

$$\mu = \cos^{-1} \frac{d}{|\underline{h}|}$$

Now the NCDs for a given LOS specified by the angle φ can be calculated by using equation (18) with r and θ given by equations (33) and (34) in the two part integral

$$NCD = \frac{A_v}{MW} \rho^* Ar^{*2} \int_{S_2}^{S_3} \frac{1}{r^2} \left\{ \cos\left(\frac{\pi}{2} \frac{\theta}{\theta_\infty}\right) \right\}^{2/(\gamma-1)} ds$$

$$+ \frac{A_v}{MW} \rho^* Ar^{*2} f(\theta_0) \int_{S_1}^{S_2} \frac{1}{r^2} \exp[-\beta(\theta - \theta_0)] ds \tag{37}$$

The constant s_3 in the upper limit of the integral above is the cutoff distance beyond which there is no significant contribution to the NCD. It is also assumed that the contribution to the total NCD for $0 \leq s \leq s_1$ is negligible.

Back flow can be estimated by looking beyond 90° at the plots for mass flux per solid angle versus angle from centerline. However, as a measure of the impact on a sensitive surface, the back flow is calculated assuming the thruster and observer are in the locations given in figure 5, located a distance h apart. Therefore, the impingement rate from back flow reaching a sensitive surface at the observer location is,

$$\frac{\left(\frac{d\dot{m}}{d\Omega}\right)_{\theta=\theta b}}{r^2} = \rho U = \rho^* A \left(\frac{r^*}{h}\right)^2 \exp[-\beta(\theta_b - \theta_o)]U \quad \frac{g}{cm^2 \cdot s} \qquad (38)$$

where

$$\theta_b = 180° - \mu$$

and

$$U = 0.5U_1 = 0.5\left(\frac{\gamma + 1}{\gamma - 1}\right)^{1/2} U^*$$

PARAMETRIC STUDIES ON NCD AND ESTIMATED BACK FLOW

Space Station Resistojet

A multipropellant resistojet propulsion system benefits the space station by providing reboost capability as well as elimination of waste gases. Using waste gases saves the significant cost of delivering propellant to and removal of wastes from the space station. The resistojet accomplishes its task by electrically heating waste gases from the space station's Environmental Control/Life Support System (ECLSS), Materials Technology Labs (MTL), and Attached Payloads in a heat exchanger and expanding it through a nozzle. Typical propellants include water, carbon dioxide, hydrogen, methane, hydrazine, argon, and nitrogen, but almost any gas generated by ECLSS or MTL can be used. In resistojets for space station application, specific impulse is traded for long life. An engineering model of a space space station resistojet [28] is shown in figure 6. For a space station resistojet producing thrusts from 0.222 to 0.890 N (0.050 to 0.200 lb_f), typical operating conditions are T_o = 300 to 1100 °C and P_o = 1.38×10^5 to 2.76×10^5 Pa (20 to 40 psia) at mass flow rates on the order of 262-872 g/hr. Specific impulses range from a high of 500 sec for hydrogen and a low of 130 sec for carbon dioxide [29]. The resistojet is physically very small with a throat diameter of 0.102 cm (0.040 in.) and at a nozzle area ratio of 100:1, its length is 1.27 cm (0.5 in.). The whole thruster is about 30.48 cm (12 in.) long and 7.62 cm (3 in.) in

diameter. In the parametric studies that follow, the baseline is a 20° half angle conical nozzle with an area ratio of 100:1 operating at T_o = 1000 °C and P_o = 2.68x10^5 Pa producing a thrust of 0.356 N using nitrogen, referred to as case 1. Case 2 is identical to case 1 except that the area ratio is changed from 100:1 to 200:1 to study the effect of increased area ratio on the plume structure. To see the effect of nozzle half angle, the nozzle in case 3 uses a half angle of 10° instead of the 20° angle used in the baseline case. The same geometrical nozzle and operating conditions are used in case 4, but the fluid is changed to hydrogen to see the effect of molecular weight on the far field expansion and resulting column densities. Finally, in case 5, the polyatomic molecule H_2O is used to study the effect of the specific heat ratio on the plume structure and column densities. Nitrogen, hydrogen and water are chosen as working fluids in the above cases because these will be the most abundant waste fluids on the space station.

Results

The results for the modified Simons analysis as applied to the five cases mentioned above are given in table II which lists the major plume parameters and operating conditions. Figures 7 to 11 are contour plots of constant number density for the five cases. A plot comparing the number densities versus angle from centerline at an axial distance of 50cm downstream from the nozzle exit plane for the five cases is given in figure 12.

The contour plots for all five cases show the highly viscous nature of the resistojet thrusters. The angle θ_0 which separates the inviscid core expansion from the boundary layer expansion is less than 20° from the centerline for all cases. Mass flow calculations for all cases show that less than 38 percent of the flow is in the inviscid core. While all cases produce a thrust of 0.356 N (0.080 lb_f), the cases using nitrogen (cases 1 to 3) have a mass flow rate of 0.242 g/sec while case 4 (H_2) has a rate of 0.073 g/sec and case 5 (H_2O) is 0.182 g/sec.

In comparison with the baseline, case 2 shows that increasing the area ratio of the nozzle, which increases the exit Mach number, results in a smaller limiting expansion angle θ_∞ from 66° in case 1 to 61° in case 2. However, the increased length of the nozzle produces a thicker boundary layer at the nozzle exit where the boundary layer is 43 percent of the exit radius for case 2 compared with 37 percent for case 1. One effect of the thicker boundary layer in case 2 is seen in the contour plot where the ratio θ_0/θ_∞ decreases from 0.26 in case 1 to 0.23, indicating a higher percentage of plume mass flow originates in the viscous portion of the nozzle flow. Looking at figure 12 showing the number density at a given axial location shows the plume produced by the higher area ratio nozzle is more concentrated around the centerline at this location.

The effect of nozzle half angle on the far field plume can be seen by comparing case 3 to case 1. Changing the nozzle half angle

from 20° to 10° results in a reduction in the limiting expansion angle from θ_∞ = 66° to 58°, even though the exit Mach number is decreased from M_e = 5.96 to 5.71 due to viscous effects. Decreasing the nozzle half angle has a greater effect on the final limiting angle θ_∞ than the increase in the Prandtl-Meyer angle for a fluid expanding from an initial Mach number 5.71 rather than 5.96 (see eq. 3). For case 3, θ_0/θ_∞ = 0.21 as compared to the value of 0.26 of case 1 and the 0.23 of case 2 which means an even higher percentage of the plume mass flow rate is found in the viscous region due to the longer nozzle length and smaller cone angle. Again looking at figure 12 shows that the plume for case 3, even though more viscous, is more concentrated around the centerline than the baseline case.

Comparing case 4 to case 1 will show the effect of molecular weight on the far field plume. Although the nozzles are producing the same thrust 0.356 N, the mass flow rate for case 4 using hydrogen is 0.073 g/s as compared to 0.242 g/s for case 1. This is because the specific impulse for H_2 is 500s while for N_2 the specific impulse is 150s. Nevertheless, the plume structure for these two cases is very similar as seen in the contour plot and in figure 12. Although the mass flow rate is lower, there are 4.2 times as many molecules per second emitted by the H_2 case than the N_2 case. This can be seen both in the contour plot in figure 10 and in figure 12 where the plots have the same shape but

the H_2 plot is displaced outward due to the fact that there are more molecules.

Finally, comparing case 5 to case 1 will show how the specific heat ratio effects the far field plume. As in the previous comparison, the thrust level is the same but the mass flow rates are different due to the difference in specific impulses (specific impulse for H_2O is 200s). The particle emission rate, however, is only 1.17 times that of case 1. The main difference between these two cases is found on inspecting the contour plot given by figure 11. It is seen that the limiting angle due to lower specific heat ratio, $\gamma = 1.33$ for H_2O, is 21 percent greater than case 1 using N_2 with $\gamma = 1.4$. Therefore, the plume number density is less concentrated around the centerline as seen in figure 12.

Column Density

Figure 13 shows the column density as a function of line of sight (LOS) angle for the five study cases. The observer is located 50 m above and 35 m behind the resistojet source, as illustrated in figure 5. For the line of sight angles, zero corresponds to the zenith LOS, 90° is the aft LOS, and 110° is the LOS angle which will intercept the earth's horizon, if the space station altitude is 463 km. Figure 14 is a blowup of the previous figure for LOS angles from 10° to 90°. Figure 15 presents the same plot as above but only for cases 1 through 3 (N_2 cases) which show the change in column density for changes in area ratio and

nozzle half angle. The column density calculations were stopped after the 110° LOS because it is assumed that a sensitive astronomical viewing instrument will avoid the LOSs which come close to or intersect the earth.

On inspecting figure 13, it is seen that all cases produce NCDs on the order of 10^{11} mol/cm^2 for LOS angles from 10° to 60°. These LOSs lie in the viscous region of the plume. At 60°, NCDs for case 4 (H_2) are slightly greater than the other cases which are all still about the same. Near the 75° LOS angle, the core flow region of the plume is seen by the observer and the column densities for each case begin to rise rapidly but at different rates. At the 110° LOS, the NCDs for the five cases range from a low of 6.1×10^{12} mol/cm^2 for case 5 and a high of 1.04×10^{13} mol/cm^2 for case 3. It is more easily seen by looking at figure 14 that except for case 4, the cases which have a higher NCD for LOS angles 10° to 75° have lower NCDs beyond the LOS angle 75°.

Figure 15 which compares only the N_2 cases at the same source flow rate shows that reducing the nozzle half angle and increasing the nozzle area ratio will reduce the NCDs for LOSs lying in the viscous region of the far field plume, but the NCDs are increased for the LOSs which intersect the core region of the plume, as compared to the baseline.

Back Flow

The back flow from the resistojet source calculated from equation (39) for the observer location specified above for the five cases is as follows:

Case 1	1.32×10^{-12} g/cm^2/s
Case 2	1.08×10^{-12} g/cm^2/s
Case 3	7.00×10^{-13} g/cm^2/s
Case 4	6.65×10^{-13} g/cm^2/s
Case 5	3.00×10^{-12} g/cm^2/s

The first three cases involving N_2 show that the back flow to the observer location decreases slightly from the baseline when the plume is kept closer to the centerline by increasing the area ratio or reducing the nozzle half angle. The difference between case 4 and case 1 is largely due to the lower nozzle mass flow rate since the plume parameters for these two cases are very similar. A major reason for case 5 producing the maximum back flow despite its lower nozzle mass flow rate is because it has the greatest limiting expansion angle.

Conclusions

The general conclusion from the column density discussion is that for the cases which confine the far field plume to near the centerline, which can be done by increasing the area ratio (case 2), decreasing the nozzle half angle (case 3), or increasing the specific heat ratio (cases 1, 2, 3, and 4 as compared to

case 5), the resulting NCDs will be less for LOSs passing through the viscous portion of the plume only.

For LOS angles which intersect the core portion of the plume, the NCDs for the confined plumes will grow rapidly and exceed the baseline case where no special attempt was made in confining the plume. However, if an astronomical observing instrument is sensitive to an induced NCD of 10^{13} mol/cm^2, the improvement in NCDs for LOSs from 10° to 75° where the induced NCDs are no greater than 1.5×10^{12} mol/cm^2 is inconsequential when compared to the NCDs seen by the observer at a LOS of 110°. At this LOS angle, case 3 with a 10° nozzle half angle produces a NCD of 1.04×10^{13} mol/cm^2 which exceeds the observer's limit while the NCD produced by the baseline case with a 20° nozzle half angle produces a NCD of only 7.95×10^{12} mol/cm^2. Specific nozzle geometries can be chosen depending on which LOSs are of interest to an observer.

In regards to the back flow calculated by extending the modified Simons' method beyond θ_∞, the nozzles which confine the plume produce slightly less backflow. In comparing the N_2 cases, the minimum backflow produced by case 3 with the reduced nozzle half angle is 1.9 times less than the baseline case. When using the same nozzle, larger boundary layers at the nozzle exit will produce higher back flow rates.

In summary, this report has presented analyses which are valuable tools that are easily and rapidly used for systems level plume and contamination studies.

REFERENCES

1. E.N. Borson, and R.V. Peterson, "Spacecraft Contamination from Propulsion Systems." Air Force Propulsion Laboratory, Edwards AFB, CA, AFRPL-TR-84-068, Oct. 1984.

2. J.P. Simpson, and F.C. Witteborn, "Effect of the Shuttle Contaminant Environment on a Sensitive Infrared Telescope." Applied Optics, vol.16, no.8, Aug. 1977, pp.2051-2073.

3. G.A. Simons, "Effect of Nozzle Boundary Layers on Rocket Exhaust Plumes." AIAA Journal, Vol. 10, No. 11, Nov. 1972, pp. 1534-1535.

4. J.E. Genovese, "Rapid Estimation of Hydrazine Exhaust Plume Interaction." AIAA Paper 78-1091, July, 1978.

5. V.S. Calia, and J.W. Brook, "Measurements of a Simulated Rocket Exhaust Plume Near the Prandtl Meyer Limiting Angle." Journal of Spacecraft and Rockets, vol.12, no.4, Apr. 1975, pp. 205-208.

6. H. Legge, and R. D. Boettcher, "Modelling Control Thruster Plume Flow and Impingement." 13th International Symposium on Rarefied Gas Dynamics, O.M. Belotserkovskii, et al., eds., New York: Plenum Press, 1982, pp. 983-992.

7. G. Dettleff, R.-D. Boettcher, C. Dankert, G. Koppenwallner, H. Legge, "Attitude Control Thruster Plume Flow Modelling and Experiments." AIAA Paper 85-0933, June, 1985.

8. H. Legge, C. Dankert, and G. Dettleff, "Experimental Analysis of Plume Flow from Small Thrusters." 14th International Symposium on Rarefied Gas Dynamics, H. Oguchi, ed., New York: Columbia Univ. Press, 1984, pp. 279-286.

9. H. Legge, and G. Dettleff, "Pitot Pressure and Heat Transfer Measurements in Hydrazine Thruster Plumes." Journal of Spacraft and Rockets, vol. 23, no. 4, July-Aug. 1986, pp. 357-362.

10. K.W. Nauman, "The Highly Underexpanded Exhaust Plume from Nozzles with Boundary Layer." Translation of DFVLR-FB-85-10, Doctor of Engineering Dissertation, University of Karlsruhe, Sept. 1985. (Also European Space Agency Report ESA-TT-929)

11. J.G. Suebold, "Use of Viscous Nozzle Flow Program and the Method of Characteristics Plume Program to Predict Plume Expansion in the Back Flow Region for Small Thrusters." JANNAF 9th Plume Technology Meeting, Chemical Propulsion Information Agency, Laurel, MD, CPIA-PUBL-277, 1976, pp. 1-14.

12. B.P. Cooper, Jr., "A Computational Scheme Usable for Calculating the Plume Backflow Region." 10th Space Simulation Conference, New York: AIAA, 1978, pp. 150-152.

13. G.A. Bird, "Breakdown of Continuum Flow in Freejets and Rocket Plumes." 12th International Symposium on Rarefied Gas Dynamics, S.S. Fisher, ed., New York: AIAA, 1980, pp. 681-694.

14. J.E. Hueser, L.T. Melfi, Jr., G.A. Bird, and F.J. Brock, "Analysis of Large Solid Propellant Rocket Engine Exhaust Plumes Using the Direct Simulation Monte Carlo Method." AIAA Paper 84 0496, Jan. 1984.

15. J.E. Hueser, L.T. Melfi, Jr., G.A. Bird, and F.J. Brock, "Rocket Nozzle Lip Flow by Direct Simulation Monte Carlo Method," Journal of Spacecraft and Rockets, vol. 23, no. 4, July Aug. 1986, pp. 363-367.

16. C.S. Guernsey, and R.D. McGregor, "Bipropellant Rocket Exhaust Plume Analysis on the Galileo Spacecraft." AIAA Paper 86-1488, June, 1986.

17. F.P. Boynton, "Exhaust Plumes from Nozzles with Wall Boundary Layers," Journal of Spacecraft and Rockets, vol. 5, no. 10, Oct. 1968, pp. 1143-1147.

18. J.A.F. Hill, and J.S. Draper, "Analytical Approximation for the Flow from a Nozzle into a Vacuum." Journal of Spacecraft and Rockets, vol. 3, no. 10, Oct. 1966, pp. 1552-1554.

19. J.S. Draper, and J.A.F. Hill, "Rarefaction in Underexpanded Flows." AIAA Journal, vol. 7, no. 7, July 1969, pp. 1400-1401.

20. F.A. Albini, "Approximate Computation of Underexpanded Jet Structure." AIAA Journal, vol. 3, no. 8, Aug. 1965, pp. 1535-1537.

21. M. Sibulkin, and W.H. Gallaher, "Far-Field Approximation for a Nozzle Exhausting into a Vacuum." AIAA Journal, vol 1., no. 6, June 1963, pp. 1452-1453.

22. G.F. Greenwald, "Approximate Far-Field Flow Description for a Nozzle Exhausting into a Vacuum," Journal of Spacecraft and Rockets, Vol. 7, No. 11, Nov. 1970, pp. 1374-1376.

23. F.P. Boynton, "Highly Underexpanded Jet Structure: Exact and Approximate Calculations." AIAA Journal, vol. 5, no. 9, Sept. 1967, pp. 1703-1704.

24. C.B. Cohen, and E. Reshotko, "The Compressible Laminar Boundary Layer with Heat Transfer and Arbitrary Pressure Gradient." NACA Report 1294, 1956.

25. C.K. Murch, J.E. Broadwell, A.H. Silver, and T.J. Marcisz, "Performance Losses in Low-Reynolds-Number Nozzles." Journal of Spacecraft and Rockets, Vol. 5, No. 9, Sept. 1968, pp. 1090-1094.

26. J.E. Chirivella, "Molecular Flux Measurements in the Back Flow Region of a Nozzle Plume," Jet Propulsion Laboratory, JPL-IM-33-620, July 1973. (Also NASA CR-133602)

27. L.M. Zana, D.J. Hoffman, L.R. Breyley, and J.S. Serafini, "An Analytical and Experimental Investigation of Resistojet Plumes." AIAA Paper 87-0399, Jan. 1987.

28. T.K. Pugmire, G.L. Cann, B. Heckert, and J.S. Sovey, "A 10,000 Hour Life Multipropellant Engine for Space Station Applications." AIAA Paper 86-1403, June, 1986.

29. E.W. Morren, M.V. Whalen, and J.S. Sovey, "Performance and Endurance Tests of a Multipropellant Resistojet for Space Station Auxiliary Propulsion." AIAA Paper 86-1435, June 1986.

TABLE I. - NOZZLE GEOMETRY AND OPERATING CONDITIONS USED IN PLUME ANALYSIS FOR CHIRIVELLA'S NOZZLES

Case	Nozzle 5		Nozzle 3	
Fluid	N2		CO2	
Specific impulse, s	64		64	
Specific heat ratio	1.4		1.29	
Nozzle geometry				
Area ratio	60		240	
Half angle, deg	15		25	
Throat radius, cm	0.127		0.064	
Length, cm	3.198		1.974	
Operating conditions				
Thrust, N	0.163		0.050	
Po, Pa	22098		22201	
To, K	294		294	
Mass flow rate, g/s	0.260		0.079	
Nozzle exit conditions				
Me	5.4		5.86	
Ue, m/s	722		643	
boundary layer thickness, cm	0.328		0.411	
displacement thickness, cm	0.244		0.297	
Plume parameters		Simons		Simons
A	2.347		1.466	
Beta	4.67	9.32	3.5	6.32
θ_0, deg	18	26	18	33
θ_∞, deg	65		88	

TABLE II. - OPERATING CONDITIONS AND GEOMETRY FOR PARAMETERIC STUDY NOZZLES

Case	1	2	3	4	5
Fluid	N2	N2	N2	H2	H20
Specific impulse, s	150	150	150	500	200
Specific heat ratio	1.4	1.4	1.4	1.4	1.33
Nozzle geometry					
Area ratio	100	200	100	100	100
Half angle, deg	20	20	10	20	20
Throat radius, cm	0.051	0.051	0.051	0.051	0.051
Length, cm	1.257	1.834	2.593	1.257	1.257
Operating conditions					
Throat Reynolds no.	7348	7348	7348	4424	5822
Thrust, N	0.356	0.356	0.356	0.356	0.356
Po, Pa	267853	267853	267853	299466	254947
To, K	1273	1273	1273	1273	1273
Mass flow rate, g/s	0.242	0.242	0.242	0.073	0.182
Nozzle exit conditions					
Me	5.96	6.69	5.71	5.77	5.38
Ue, m/s	1524	1542	1515	5669	1981
boundary layer thickness, cm	0.185	0.310	0.231	0.218	0.193
displacement thickness, cm	0.142	0.249	0.175	0.168	0.140
Plume parameters					
A	2.293	2.651	2.992	2.201	1.673
Beta	4.45	4.51	4.71	4.08	3.81
θ_0, deg	17	14	12	15	19
θ_∞, deg	66	61	58	67	80

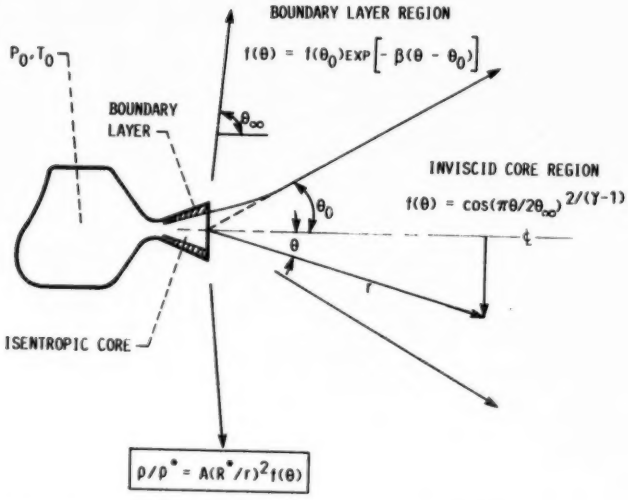

FIGURE 1. - PLUME STRUCTURE BASED ON FAR FIELD APPROXIMATION.

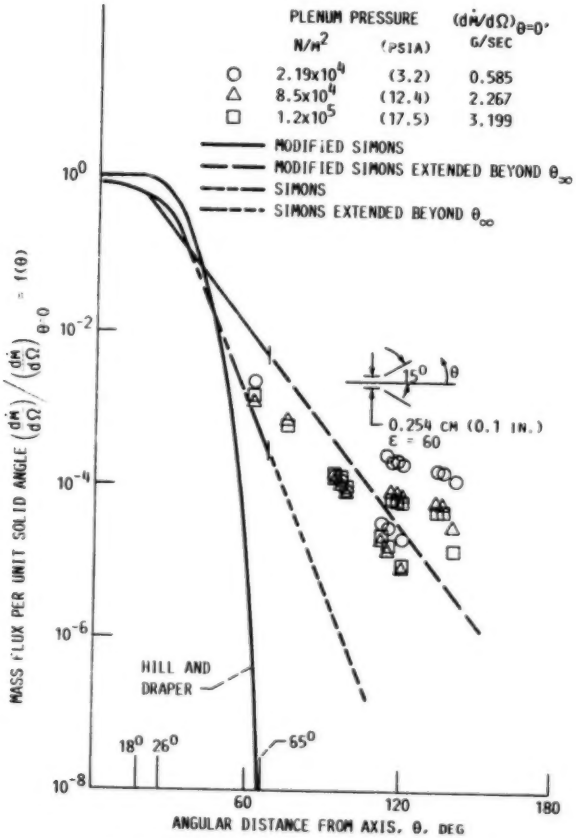

FIGURE 2. - MASS FLUX MEASUREMENT DATA REDUCED AND COMPARED WITH THE HILL AND DRAPER APPROXIMATION AND THE SIMONS AND MODIFIED SIMONS METHODS FOR NOZZLE 5, N_2 GAS, AND TEMPERATURE OF 294 K.

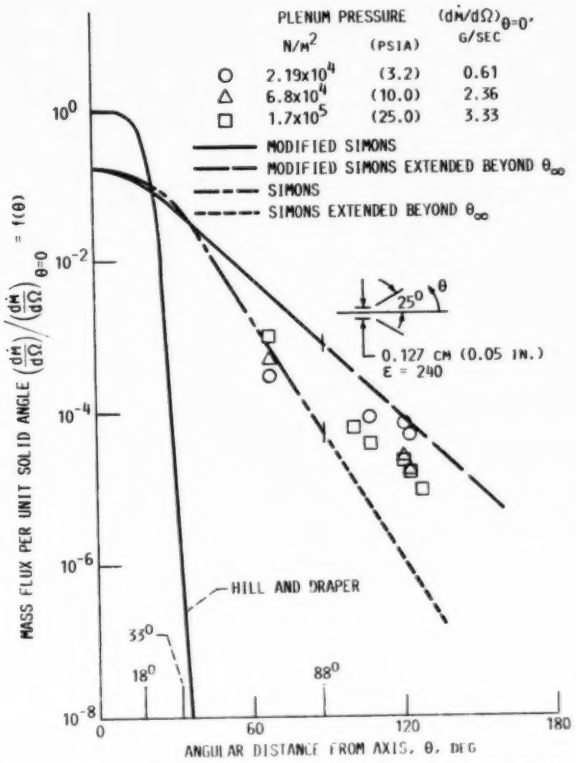

FIGURE 3. - MASS FLUX MEASUREMENT DATA REDUCED AND COMPARED WITH THE HILL AND DRAPER APPROXIMATION AND THE SIMONS AND MODIFIED SIMONS METHODS FOR NOZZLE 3, CO_2 GAS, AND TEMPERATURE AT 294 K.

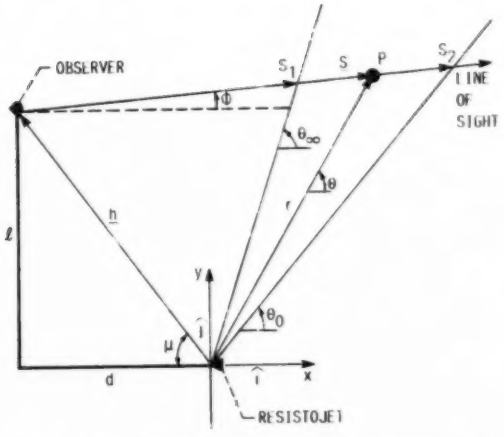

FIGURE 4. - VECTOR DIAGRAM OF RESISTOJET SOURCE AND OBSERVER LOCATIONS.

ORIGINAL PAGE IS
OF POOR QUALITY

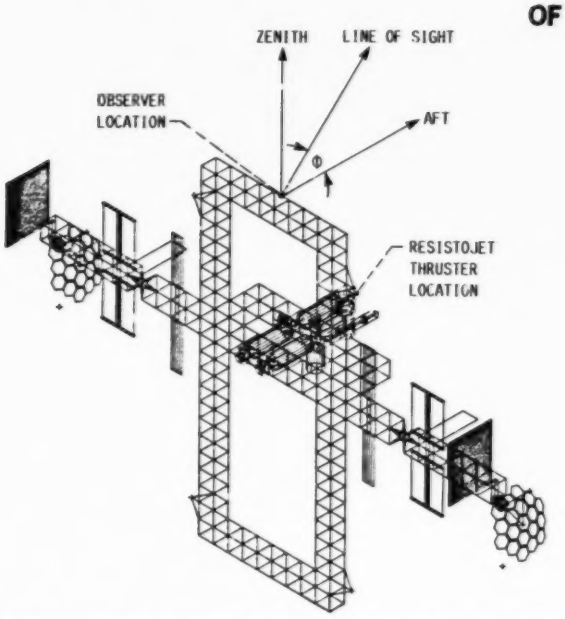

FIGURE 5. - SPACE STATION RESISTOJET AND OBSERVER LOCATIONS FOR NUMBER COLUMN DENSITY CALCULATIONS.

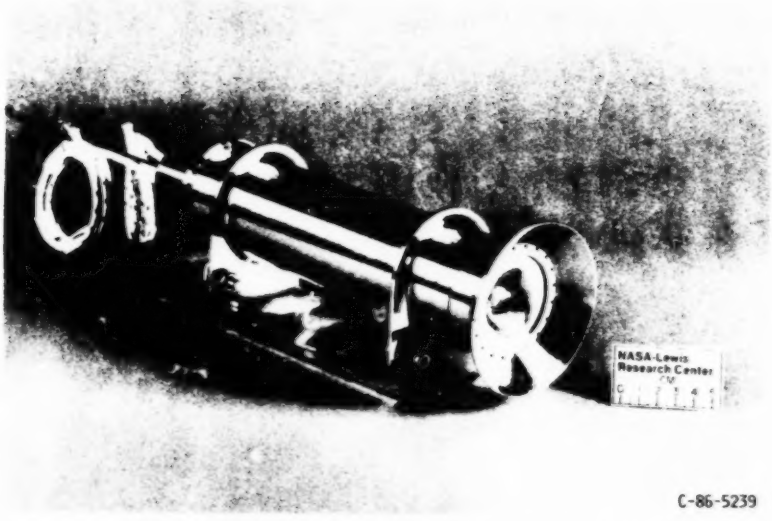

C-86-5239

FIGURE 6. - ENGINEERING MODEL RESISTOJET DEVELOPED FOR SPACE STATION APPLICATIONS.

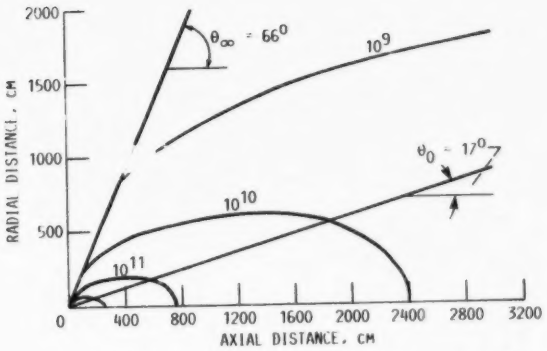

FIGURE 7. - ISODENSITY CONTOURS: CASE 1. NUMBER DENSITY, MOLECULES/CM^3.

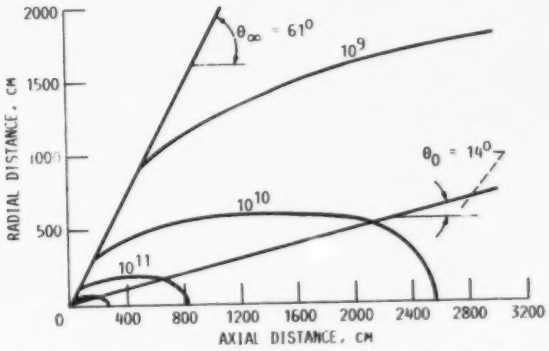

FIGURE 8. - ISODENSITY CONTOURS: CASE 2. NUMBER DENSITY, MOLECULES/CM^3.

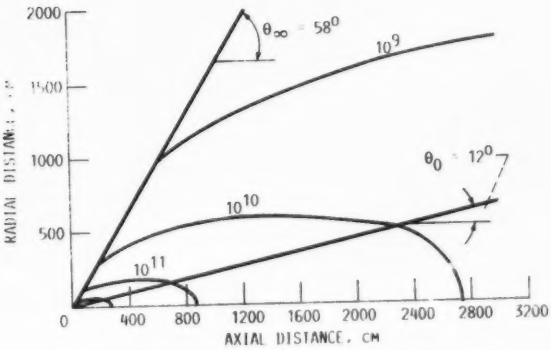

FIGURE 9. - ISODENSITY CONTOURS: CASE 3. NUMBER DENSITY, MOLECULES/CM^3.

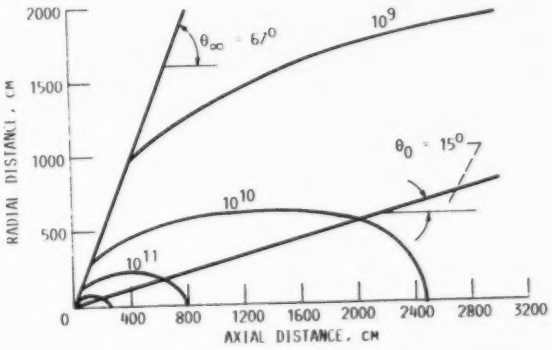

FIGURE 10. - ISODENSITY CONTOURS: CASE 4. NUMBER DENSITY, MOLECULES/CM^3.

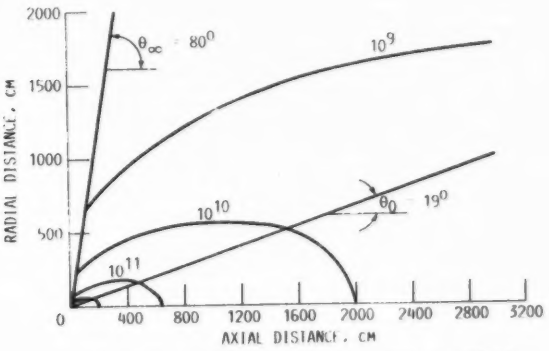

FIGURE 11. - ISODENSITY CONTOURS: CASE 5. NUMBER DENSITY, MOLECULES/CM^3.

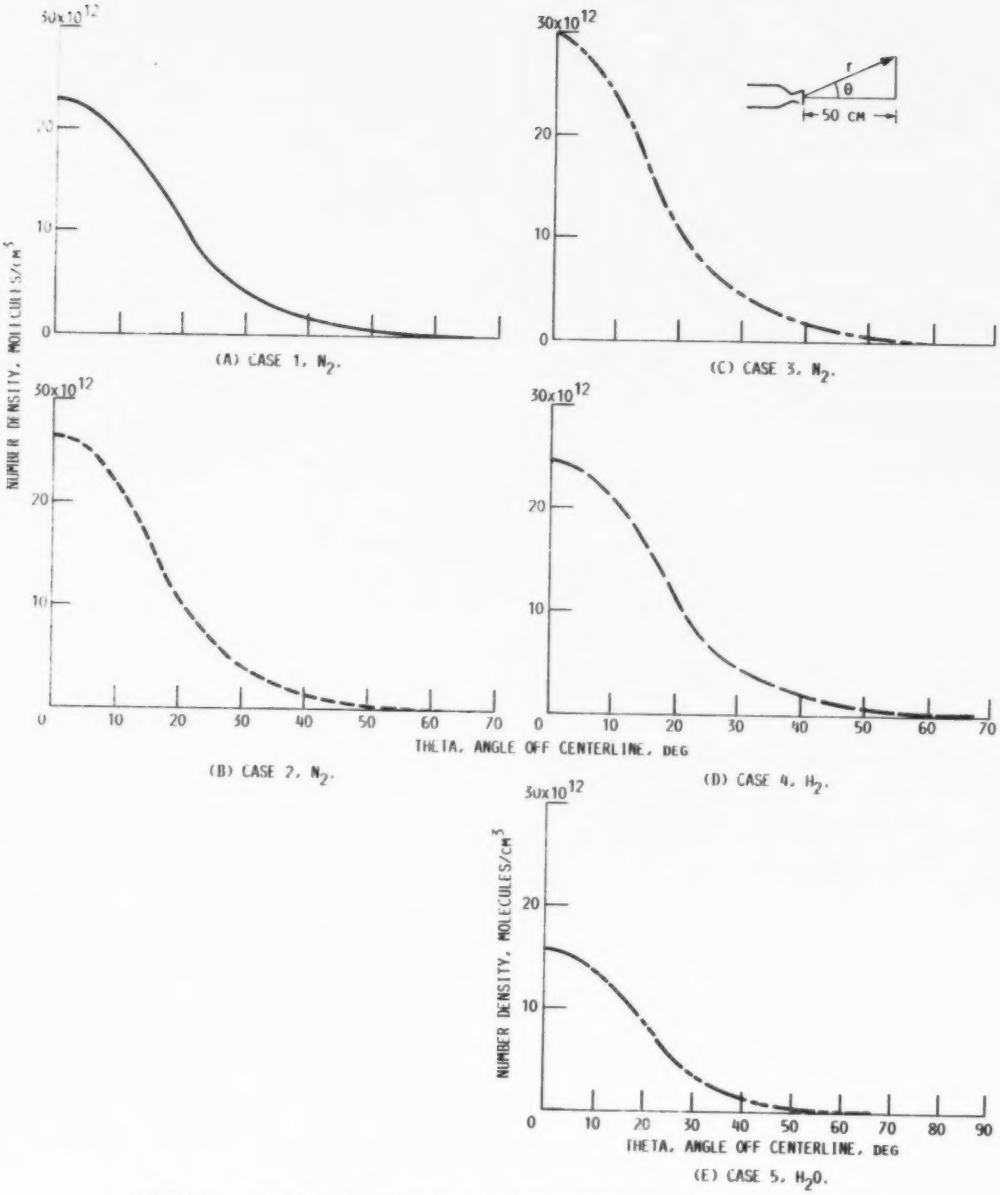

FIGURE 12. - PLUME NUMBER DENSITY AT AN AXIAL LOCATION AT 50 cm FROM NOZZLE EXIT PLANE.

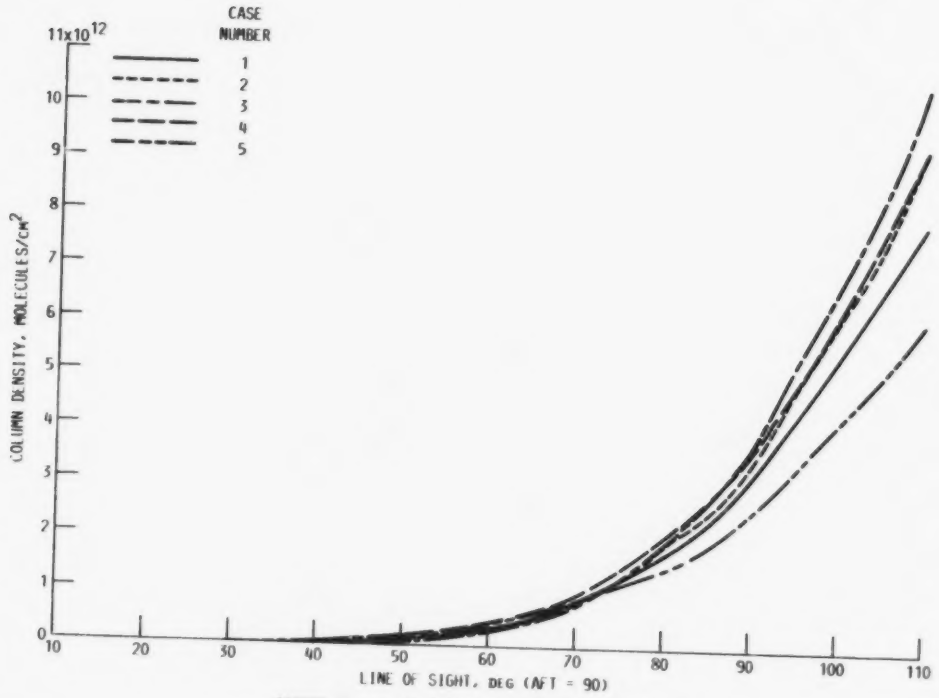

FIGURE 13. - COLUMN DENSITY VERSUS LINE OF SIGHT.

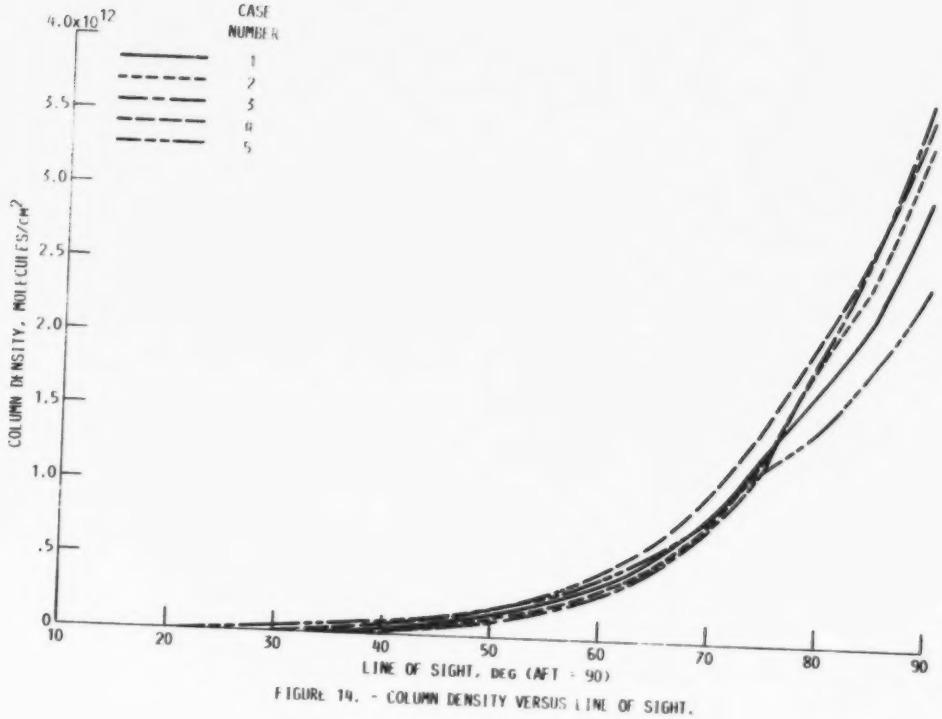

FIGURE 14. - COLUMN DENSITY VERSUS LINE OF SIGHT.

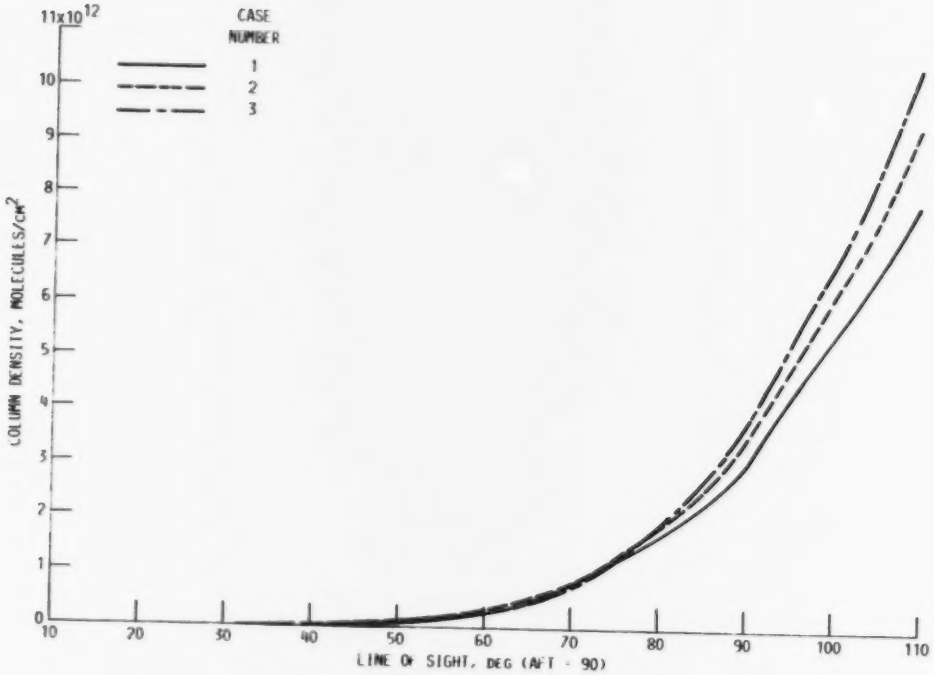

FIGURE 15.- COLUMN DENSITY VERSUS LINE OF SIGHT.

1 Report No.	2 Government Accession No.	3. Recipient's Catalog No.
NASA TM-88957		

4 Title and Subtitle	5. Report Date
Resistojet Plume and Induced Environment Analysis	May 1987
	6. Performing Organization Code: 481-02-02

7. Author(s)	8. Performing Organization Report No.
David J. Hoffman	E-3410
	10. Work Unit No.

9. Performing Organization Name and Address	11. Contract or Grant No.
National Aeronautics and Space Administration Lewis Research Center Cleveland, Ohio 44135	13. Type of Report and Period Covered: Technical Memorandum
12. Sponsoring Agency Name and Address	14. Sponsoring Agency Code
National Aeronautics and Space Administration Washington, D.C. 20546	

15. Supplementary Notes

This report was a thesis submitted in partial fulfillment of the requirements for the degree Master of Science to Case Western Reserve University in 1987.

16. Abstract

The source flow method developed by G.A. Simons for calculating the far field plume density produced by high thrust rocket nozzles is modified and applied to low thrust resistojet nozzles with Reynolds numbers on the order of 4000 to 7000. Simons' original method and the modified analysis are compared to mass flux measurements taken by Chirivella in a JPL vacuum tank facility. Results of the comparison show the modified analysis presented in this paper more accurately predicts the mass flux at large angles from the nozzle centerline than Simons' original method. The modified Simons analysis is then used to calculate the plume structure and two contamination parameters, number column density and back flow, for five nozzle geometries representative of Space Station resistojets.

17. Key Words (Suggested by Author(s))	18. Distribution Statement
Exhaust plumes contamination Space Station resistojets	Unclassified - unlimited STAR Category 20

19. Security Classif. (of this report)	20. Security Classif. (of this page)	21. No. of pages	22. Price*
Unclassified	Unclassified	53	A04

*For sale by the National Technical Information Service, Springfield, Virginia 22161